JOURNAL OF CATALYSIS 124, 451–464 (1990)

Oxidative Coupling of Methane on Alkali Metal-Promoted Nickel Titanate

I. Catalyst Characterization and Transient Studies

E. MIRO,[1] J. SANTAMARIA,[2] AND E. E. WOLF[3]

Chemical Engineering Department, University of Notre Dame, Notre Dame, Indiana 46556

Received October 18, 1989; revised February 6, 1990

Nickel titanate, a mixed oxide with ilmenite structure, develops activity for methane oxidative coupling reaction upon promotion with alkaline metals (Li, Na, K). Typically, higher hydrocarbon yields of ca. 13% with ca. 70% selectivity can be obtained with a 9.7% $Li/NiTiO_3$ catalyst and C_2 + yields of ca. 8% with ca. 60% selectivity with a 22% $Na/NiTiO_3$ catalyst. Transient experiments involving steps, pulses, and steady-state isotopic switches indicate that while on a 9.7% $Li/NiTiO_3$ catalyst the activity is mainly related to lattice oxygen, there is little lattice oxygen involvement in oxidative coupling over sodium-loaded nickel titanate. Isotopic switch results revealed that carbon dioxide interacts strongly with both lithium- and sodium-promoted surfaces, but the concentration of long-lived adsorbed methane is too low to be differentiated from the interaction of argon with the surface. X-ray diffraction and BET results indicate that increasing the degree of alkali metal loading lowers the surface area and creates different phases after pretreatment at elevated temperatures. X-ray photoelectron spectroscopy revealed that different types of carbon and oxygen species are present on the surface.

INTRODUCTION

In the past decade, methane oxidative coupling to ethane, ethylene, and higher hydrocarbons has attracted the attention of many laboratories, as evidenced by the number of review papers on the subject (*1–5*). In spite of this effort, many aspects of the catalyzed process are not yet well understood, and the highest C_2 yields reported to date in the literature (about 20%) are still too low to make the process commercially feasible.

Previous work in our laboratory has been focused on the role of gas-phase and surface oxygen in the oxidative coupling process. Lane and Wolf (*6*) showed that noncatalyzed gas-phase reactions become important at high reactant partial pressures, high residence times, methane-to-oxygen ratios lower than 3, and temperatures above 650°C. Subsequent studies investigated the catalytic aspects of the reaction on Li/TiO_2 (*7*) and on various titanate catalysts (*8*). In these studies, it was found that a catalyst of 16.2 wt% lithium over titania gave hydrocarbon yields as high as 12.5%, and that a lanthanum–titanate catalyst was capable of activating methane at temperatures much lower than those of the other titanates studied.

There seems to be general agreement in the literature that the mechanism of ethane formation is the abstraction of hydrogen from methane, followed by the release of methyl radicals to the gas phase, which are then coupled to form ethane (*9–11*). The same consensus is not found for the nature of the methane interaction with the catalyst surface, the role of the different oxygen species present in the catalyst, and the mecha-

[1] On leave from the Department of Chemical Engineering, University of Zaragoza, 5009 Zaragoza, Spain.

[2] On leave from INCAPE, Universidad Nacional del Litoral, Sgo. del Estero 2829, 3000 Santa Fe, Argentina.

[3] To whom correspondence should be addressed.

0021-9517/90 $3.00

nism of ethylene and carbon oxides formation, which most probably vary with the type of catalyst used. In fact, in a previous paper (*12*) we have reported that the role of the oxygen stored on lithium-promoted titanate catalysts varies depending on whether lithium is supported on titania, nickel titanate, or lanthanum titanate. These results indicated that the mobility and the amount of the oxygen species on the catalyst surface are key factors in determining the activity and selectivity of a catalyst.

Several authors (*13–15*) have studied catalysts in which the lattice oxygen appears to be active, resulting in high selectivity toward higher hydrocarbons. The catalytic reaction of methane with adsorbed oxygen has also been reported in a variety of catalysts (*16–18*). Previous work (*12*) in our laboratory showed that $Li/NiTiO_3$ was an active and selective catalyst for methane dimerization, mainly via the participation of lattice oxygen. On the other hand, other results obtained in our laboratory indicated that when $NiTiO_3$ was loaded with Na instead of with Li, some mechanistic aspects of the reaction changed. Given these results, a systematic comparative study of both catalysts was undertaken in order to characterize their behavior and to gain some insight into the effect of the Li and Na promoters on the mechanism by which the oxidative coupling of methane takes place on nickel titanate (ilmenite). To this end, transient experiments using pulse and step functions, as well as isotopic tracers, have been carried out together with the characterization of the catalysts by means of XRD, XPS, and BET techniques.

EXPERIMENTAL

Catalyst preparation and pretreatment. The catalysts were prepared from the mixed oxide nickel titanate (Alfa Products, 99.7% purity $NiTiO_3$ basis), which was impregnated with a solution of either lithium oxide or sodium carbonate in deionized water. Change of the Li precursor salt to lithium carbonate did not affect the results, and catalyst characterizations indicate that in both cases the main phase present is the carbonate phase. The slurry was heated to 50°C and the water was evaporated with stirring until a dry powder was obtained. Each catalyst was calcined first at 650°C in flowing air for 5 h and then at 750°C for 2 h. The amount of alkali metal loading is defined as the ratio of the initial weight of lithium or sodium divided by the initial total weight of the catalysts. While the effect of loading was studied first and is presented in a subsequent paper (*19*), the detailed characterization and transient studies are presented for catalysts with a lithium loading of 9.7% and a Na loading of 22% since these catalysts gave the highest yield under the conditions studied. Reference is also made to a catalyst with 1.6% Na loading since detailed kinetic data for this catalyst were available. The catalysts are denoted in the text by the loading figure preceding $Li/NiTiO_3$ or $Na/NiTiO_3$.

Apparatus and procedure. Steady-state kinetic experiments were performed using a single-pass flow reactor made of fused-silica with an inside diameter of 0.95 cm and a heated length of 15 cm. The details of this apparatus have been given elsewhere (*6–8*). Depending on the catalyst, the amounts charged in the reactor varied between 0.25 and 1.0 g, and the flow rates varied in the range 50 to 150 cm^3/min. Experimental conditions were selected to minimize gas-phase reactions; i.e., the reactant partial pressure $(P_{O_2} + P_{CH_4})/P_{total}$ was less than 0.4 and the residence times were less than 0.1 min.

A schematic diagram of the apparatus used for the transient experiments is shown in Fig. 1. The reactor consisted of a 2-mm-i.d. quartz tube reactor, especially designed to minimize dead volume. A combination of three-way solenoid valves, six-port valves, and a 16-loop valve (Valco) was used to generate either step or pulse functions in the methane and/or oxygen feeds. The reaction products in the effluent stream were analyzed by a gas chromatograph equipped with Carbosphere and HayesSep Q packed col-

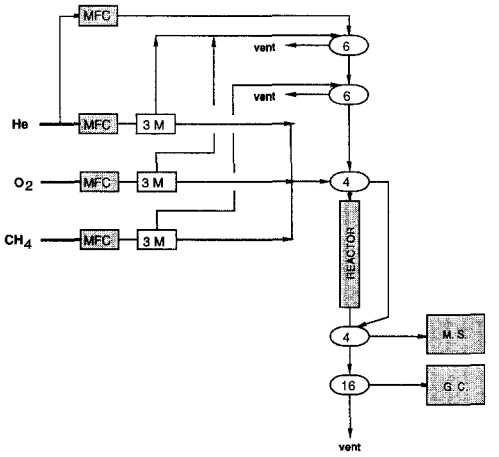

FIG. 1. Diagram of the apparatus for transient and steady-state experiments. MFC, mass flow controllers; 3M, three-way solenoid valves; 6, sampling valves; 4, four-way valves; 16, 16-loop sampling valve; MS, mass spectrometer; GC, TCD–FID gas chromatographic system.

umns and TCD/FID detectors. Alternatively, the exit stream could also be directed to a UTI-100-C quadrupole mass spectrometer equipped with a fast-response continuous sampling system. Mass-to-charge ratios of 4, 15, 26, 28, 29, 30, 32, and 44 were used for the analysis of He, O_2, CO, CO_2, CH_4, C_2H_6, and C_2H_4 after appropriate calibration. In addition, in experiments involving isotopic tracing with either $^{13}CH_4$ or $^{18}O_2$, mass-to-charge ratios of 17, 34, 36, 40, 46, and 48 were scanned to monitor $^{13}CH_4$, $^{16}O^{18}O$, $^{18}O_2$, Ar, $C^{16}O^{18}O$, and $C^{18}O_2$. The fragmentation patterns for some of these components overlap considerably; therefore, a system of algebraic equations had to be solved whenever quantitative measurements of concentration for selected species are reported.

Two types of transient experiment were conducted—step and pulse input experiments. The reactor was first heated to the desired temperature while helium at a flow rate of 60 cm^3/min was introduced, and then maintained at the reaction temperature for 2 h. In the step mode the three-way valve was switched to the selected stream (i.e., methane or methane/O_2) and maintained in that position while the effluent products were collected at 5–20 s in the various loops of the multiloop sampling valve for later GC analysis.

In the pulse mode, a pulse containing one or more reactants was injected via the six-port valve into the reactor, and the effluent was either directed into the GC for separation and detection via the TCD or FID detectors, or directly analyzed using the mass spectrometer. The pulses were injected at 30-min intervals to allow for sample degassing under the He stream.

Typically, the transient experiments were carried out at 750°C, with the reactor loaded with 50–200 mg catalyst and with flow rates between 30 and 60 cm^3/min. Blank experiments under these conditions yielded negligible methane conversion.

The reactant and carrier gases used were ultrahigh purity grades obtained from Linde Specialty Gases with the following purities: CH_4 (99.97%), O_2 (99.99%), and He (99.999%). An oxygen trap was also used in order to purify the helium. $^{13}CH_4$ (99.3%) and $^{18}O_2$ (98.3%) were obtained from Isotec.

Catalyst characterization. The BET area of each catalyst was measured after calcination but prior to reaction by a Quantachrome QS-8 unit, using the flow adsorption method, with N_2 as the adsorbing gas and helium as the carrier gas. X-ray diffraction patterns were measured using a Philips diffractometer with Cu Kα radiation, a 3° beam slit, and a 0.2° detector slit. The XRD samples were obtained using pressed wafers of the catalyst which were mounted on glass slides. XPS characterization was carried out on fresh samples and also after 50 h of time on stream using a Surface Science XPS spectrometer at the Amoco Research Center.

RESULTS

Steady-state activity and selectivity. Unpromoted $NiTiO_3$ was found to be almost inactive for the methane oxidative coupling reaction, giving conversions and selectivities similar to those observed for the noncat-

TABLE 1

Methane Conversion, Higher Hydrocarbon Selectivity, and Higher Hydrocarbon Yield Results for the Alkali Metal-Promoted Nickel–Titanate Catalysts

Catalyst[a]	Reaction conditions			CH_4 conversion	C_{2+} selectivity	C_{2+} yield
	T(°C)	W(g)	CH_4/O_2			
$NiTiO_3$	800	1.0	2.0	4.9	59.5	2.9
1.6% Na	800	1.0	2.0	22.0	38.0	8.4
1.6% Na	850	1.0	2.0	39.0	41.3	16.1
22% Na	750	0.25	4.0	12.7	60.1	7.6
22% Na	800	0.25	4.0	22.1	61.5	13.6
0.5% Li	800	1.0	2.0	20.1	49.1	9.9
0.5% Li	850	1.0	2.0	35.5	47.0	16.7
9.7% Li	750	0.25	4.0	18.9	69.7	13.2
9.7% Li	800	0.25	2.0	38.2	46.6	17.8

[a] After 2 h of time-on-stream.

alyzed gas-phase reaction. The promotion of $NiTiO_3$ with either Li_2O or Na_2CO_3 increased both methane conversion and the hydrocarbon yield. Table 1 displays results of the activity and selectivity at 750 and 800°C obtained with the various catalysts prepared. Additional detailed kinetic studies are presented in a subsequent paper (*19*). Table 1 shows that for both Li and Na catalysts the hydrocarbon yield increased as the alkali metal loading was increased from 1.6 to 22% for Na and from 0.5 to 9.7% for Li. The optimum yield that can be attained using the catalysts with higher loadings is of the order of 23%. The purpose of the studies reported here, however, was not to optimize the yield or to develop catalysts more active than those reported in the literature, but to gain some understanding of the effect of additives in promoting the $NiTiO_3$ materials.

Step experiments. In step experiments (Fig. 2), after degassing the catalyst for 15 min, at time equal zero, pure methane was fed into the reactor for $t_1 = 30$ s. At t_1 the pure methane step was stopped and replaced by a second step containing a mixture of methane and 2% O_2. At t_2 both methane and oxygen flows were switched back to a pure He stream. The delay time (τ), indicated at the bottom of both figures, corresponds to the residence time of the gas on the line.

The results for the 9.7Li/$NiTiO_3$ catalyst (Fig. 2a) show that when the pure methane step is contacted with the surface, considerable amounts of ethane and ethylene are produced. The shape of the C_2-vs-time curve has a maximum due to the depletion of the oxygen supplied to the surface from the lattice. In the second step containing methane and oxygen, the activity increases again as oxygen is restored from the gas phase.

In the catalyst containing Na as a promoter instead of Li, a different behavior is observed as shown in Fig. 2b for the 22Na/$NiTiO_3$ catalyst. It can be seen that in this case, during the pure methane step, only small amounts of both hydrocarbons and deep oxidation products are produced. When the second methane plus oxygen step was introduced, the concentrations of all the products increased significantly. The behavior of the 1.6Na/$NiTiO_3$ was similar to that shown in Fig. 2b, although in this case, during the second step, ethane and ethylene production increased between 2 and 5 times with respect to those obtained in the first

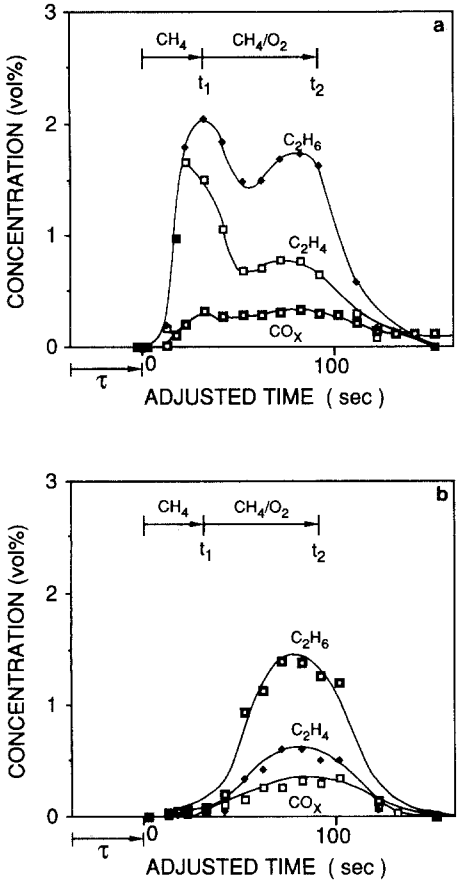

FIG. 2. Reactivity of lattice and adsorbed oxygen after out-of-phase step changes in CH_4 and O_2 over 500 mg of (a) 9.7% $Li/NiTiO_3$ and (b) 22% $Na/NiTiO_3$ at 750°C; total flow rate, 32 cm^3/min; oxygen concentration during the second step, 2%. τ is the response delay time, t_1 is the duration of the pure methane step, and t_2–t_1 the duration of the methane/oxygen step.

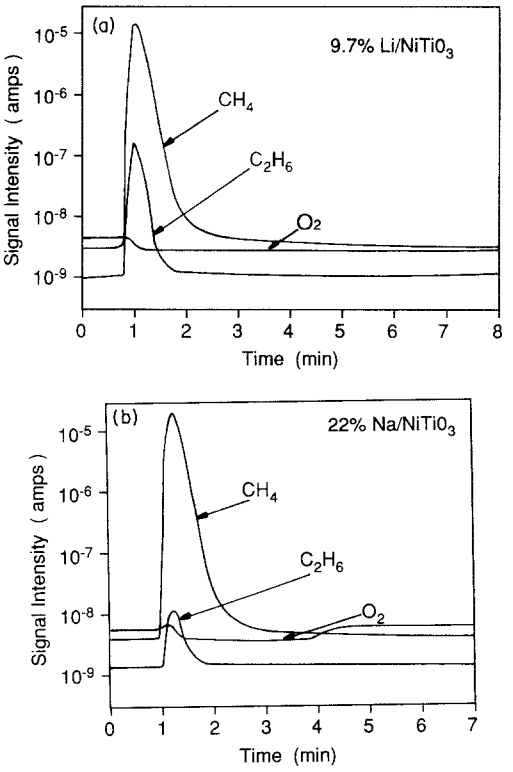

FIG. 3. Continuous mass spectrometry monitoring of selected species. Methane pulses on a controlled oxygen trace over 100 mg of (a) 9.7% $Li/NiTiO_3$ and (b) 22% $Na/NiTiO_3$. T = 750°C; helium flow rate, 60 cm^3/min.

step, instead of the 10 and 30 times corresponding increase observed on 22Na/$NiTiO_3$.

Methane pulses on a controlled oxygen trace. This technique also permits one to ascertain the role of lattice oxygen (*12*). It consists of feeding a He stream containing a trace of oxygen (typically 2 to 5 ppm) into the reactor and then using mass spectrometry to monitor the oxygen level in the exit gases after feeding one or more methane pulses. Figures 3a and 3b display the results obtained in these experiments for the 9.7Li/$NiTiO_3$ and the 22Na/$NiTiO_3$ catalysts, respectively. For simplicity, only the current signals at m/e = 15, 30, and 32 are shown, which under the conditions used are representative of CH_4, C_2H_6, and O_2, respectively. It can be observed that for the 9.7Li/$NiTiO_3$ catalyst the oxygen level in the gases exiting the reactor is depleted following the methane pulse, and considerable amounts of C_2 hydrocarbons appear almost simultaneously with the methane pulse. Furthermore, the oxygen level does not return to its initial values immediately, but it increases slowly, indicating that it is being absorbed by the catalyst to replace its lattice oxygen. Li-promoted catalysts containing smaller Li

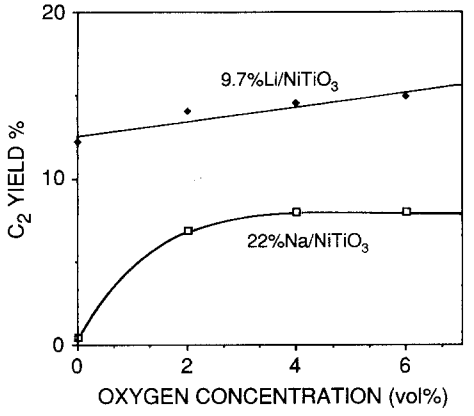

FIG. 4. C_2 yield in pulses with different oxygen concentrations over 100 mg of 9.7% Li/$NiTiO_3$ and 22% Na/$NiTiO_3$ at 750°C. Helium flow rate, 60 cm^3/min; methane concentration in the pulses, 32%.

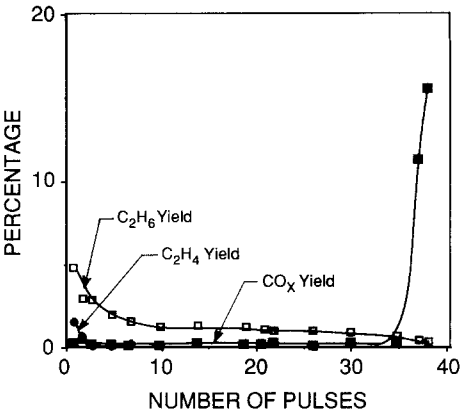

FIG. 5. Availability of lattice oxygen of the 9.7% Li/$NiTiO_3$ catalyst. Methane pulses over 100 mg of catalyst at 750°C. Helium flow rate, 60 cm^3/min.

loadings resulted in much smaller amounts of C_2 production and almost no oxygen depletion. Figure 2b shows the response of the 22Na/$NiTiO_3$ to the same experiment. It can be noted that the amount of ethane produced is much smaller and that the oxygen curve shows no long-term depletion. These results indicate that for this catalyst lattice oxygen is not depleted by methane and thus it does not participate to a large extent in the reaction. Similar results were obtained for the 1.6Na/$NiTiO_3$ catalysts.

Methane–oxygen pulses. To investigate further the role of lattice oxygen on these catalysts, pulses containing a fixed concentration of methane in mixtures of methane, oxygen, and helium were used. Pulse experiments have been previously utilized by Lo *et al.* (*20*) to study the role of different oxygen species in methane oxidative coupling over antimony-based catalysts. In Fig. 4, the C_2 yield (ethane plus ethylene) is plotted versus the oxygen concentration in the pulses. For both 9.7Li/$NiTiO_3$ and 22Na/$NiTiO_3$ catalysts, C_2 production increases with increasing oxygen concentration. However, C_2 production was negligible for the 22Na/$NiTiO_3$ when no oxygen was present in the pulse, which again indicates that the lattice oxygen is not available for reaction on sodium-promoted catalysts. The amount of CO and CO_2 detected in these pulse experiments was very small, most probably due to the strong adsorption of CO_2 on the surface.

The ability of the 9.7Li/$NiTiO_3$ catalyst to exchange its lattice oxygen was further tested in an experiment designed to deplete lattice oxygen using a series of 4.7-cm^3 pure methane pulses without exposure to oxygen between pulses. Figure 5 shows the hydrocarbon and CO_x yields with each pulse. It can be observed that the C_2H_6 yield decreases rapidly during the first 10 pulses, then very slowly during the next 25 pulses, while ethylene ceases to be detected after only 3 pulses. After 35 pulses, a large increase in methane conversion, which coincides with a similar increase in CO production and a large increase in the hydrogen concentration of the exit gases (not shown), is observed. At this point, the catalyst selectivity strongly decreases, due to the reduction of a significant fraction of the Ni on the catalyst surface.

The degree of oxygen depletion can be estimated by titrating the catalyst using oxygen pulses until the trace oxygen concentration recovers its initial value. If we assume that 1 m^2 of surface contains 6×10^{18} oxygen atoms regardless of the crystallographic

structure and the exact representation of the surface (*21*), then the amount of oxygen consumed in the reoxidation would represent approximately 70 monolayers, or equivalently, a reduction of about 6% of the Ni present in the sample. However, metal reduction occurred during the last two pulses in the previous experiment; consequently, part of the oxygen was used to reoxidize the metal, and thus the amount of oxygen available for the coupling reaction is likely to be considerably less than 70 monolayers.

In a related experiment, a 50% CH_4/He mixture was passed over the 9.7Li/$NiTiO_3$ catalyst to reduce the catalyst continuously, without allowing time between pulses which could permit oxygen transfer from the bulk to the surface. In this experiment the catalyst lost its selectivity within 2 min of reaction time, corresponding to only about one-third of the amount of methane fed to the reactor in the first 35 pulses of the previous experiment.

Isotopic oxygen tracing. ^{18}O tracing on fresh 9.7Li/$NiTiO_3$ catalyst was used in an attempt to differentiate the roles played by the different oxygen species present during reaction. Figure 6a shows the current signals at m/e = 32, 34, and 36 when a pulse of $^{18}O_2$ in a He carrier stream was sent directly to the mass spectrometer, while Fig. 6b shows the response when the same pulse was passed over 100 mg of the catalyst at 750°C. In Fig. 6b it can be seen that most of the $^{18}O_2$ signal (m/e = 36) disappears, while the signals corresponding to $^{16}O_2$ and $^{16}O^{18}O$ (m/e = 32 and 34, respectively) increase accordingly. Therefore, even in the absence of chemical reaction at 750°C there is an active exchange of oxygen between the gas phase and the 9.7Li/$NiTiO_3$ catalyst surface. On the other hand, the Na-promoted catalysts (1.6 and 22% loadings) showed little activity for isotopic oxygen exchange; i.e., similar responses (not shown) were obtained for different oxygen species, irrespective of whether the pulse was passed over the catalyst or fed directly into the mass spectrometer. Thus, in contrast with

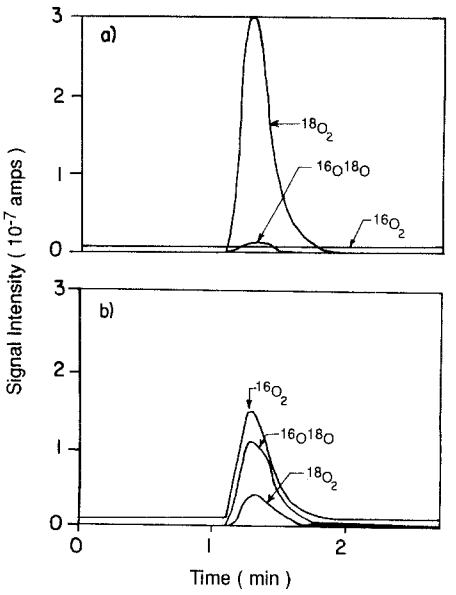

FIG. 6. Mass spectrometry monitoring of selected species. ^{18}O tracing on 100 mg of 9.7% Li/$NiTiO_3$ at 750°C; helium flow rate, 60 cm^3/min; oxygen concentration in the pulses, 7.5%. (a) Blank run, (b) catalytic run.

the results shown above for the 9.7/Li/$NiTiO_3$ catalyst, the lack of isotopic oxygen exchange for the Na-promoted catalyst further corroborates that oxygen stored in the lattice does not significantly contribute to methane activation.

Methane interaction with the catalyst surface. $CH_4/^{13}CH_4$ switches on a He carrier gas stream were used to investigate the interaction of methane with the catalyst surface under steady-state reaction conditions (see Refs. (*20, 22*)). For the $CH_4/^{13}CH_4$ switching experiment, a mixture of CH_4, Ar, and O_2 was first reacted over the catalysts at 750°C until the constant current intensities for the different m/e ratios in the mass spectrometer were reached, indicating steady-state conditions. The reacting mixture was then switched to a $^{13}CH_4$/He/O_2 mixture of the same methane and oxygen concentrations using a four-way valve. The evolution (as normalized concentrations) of both CH_4 species, Ar, and CO_2 during the CH_4 switch experiment on a 9.7Li/$NiTiO_3$

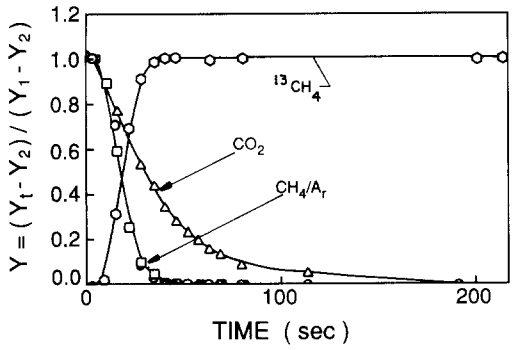

FIG. 7. Steady-state isotopic transient–kinetic analysis. Switch from ($^{13}CH_4$ + Ar + O_2) to (CH_4 + He + O_2) over 100 mg of 9.7% Li/$NiTiO_3$ at 750°C. Helium flow rate, 60 cm^3/min; CH_4/O_2 = 4. Y, Normalized concentration; Y_t, concentration at time equal t; Y_2, initial concentration; Y_1, final concentration.

is shown in Fig. 7. It can be seen that the CH_4 and Ar signals decay almost simultaneously, and that the $^{13}CH_4$ curve increases almost symmetrically with the CH_4 decay curve. This indicates that no long-lived adsorbed methane is present in significant quantities on the surface of this catalyst to be detected via this experiment. On the other hand, the carbon dioxide signal shows long relaxation times, which is to be expected in view of the large pool of surface carbonates revealed by XPS analysis. The results are the same for the Na-promoted catalysts.

Reactivity of the hydrocarbon products. In order to ascertain the reaction pathway of deep oxidation products, pulses containing mixtures of a given hydrocarbon with varying oxygen concentrations were passed over the catalysts. The 1.6Na/$NiTiO_3$ catalyst was chosen for this study, since it shows lower selectivities toward hydrocarbon product formation and did not exhibit the interference caused by strong adsorption of carbon oxides found in the catalysts with higher alkali loadings. Figures 8a–8c compare the effluent concentrations of the various products obtained using methane, ethane, and ethylene feed respectively, versus the oxygen content of the pulses.

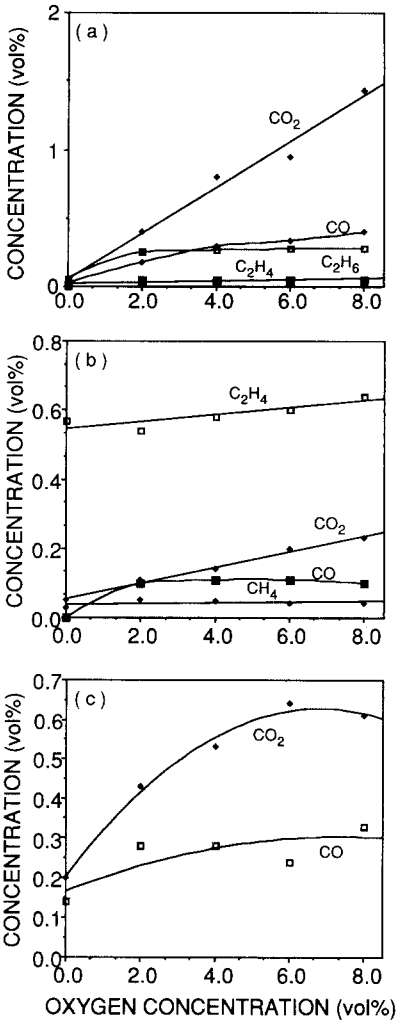

FIG. 8. Methane and product hydrocarbon pulsing at various oxygen concentrations over 100 mg of 1.6% Na/$NiTiO_3$ catalyst at 750°C. Helium flow rate, 60 cm^3/min. (a) Methane pulsing, (b) ethane (4.5% in helium) pulsing, (c) ethylene (4.5% in helium) pulsing.

When methane plus oxygen pulses (Fig. 8a) were fed, the hydrocarbon concentration increased until the oxygen concentration in the pulses reached 2% and leveled off thereafter. The major product was CO_2 and its yield increased continuously with the amount of oxygen in the pulses. Accordingly, the selectivity to hydrocarbons decreased from 80% in the pure methane pulse to 30% when 8% oxygen was included in

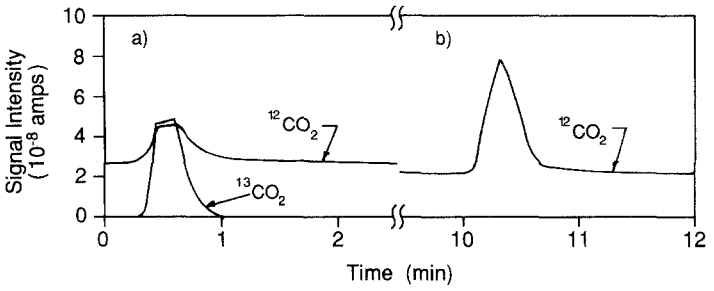

FIG. 9. Mass spectrometry monitoring of selected species. CO_2 formation from CH_4 + C_2H_6 pulses over 100 mg of 1.6% $Na/NiTiO_3$ at 750°C. Helium flow rate, 60 cm^3/min. (a) Pulse of 22.2% CH_4, 2.2% C_2H_6, and 8.9% O_2 (in helium). (b) Pulse of 22.2% $^{13}CH_4$, 2.2% C_2H_6, and 8.9% O_2 (in helium).

the pulses. When ethane/O_2 pulses (Fig. 8b) were fed, the main product was ethylene, with lower amounts of CO, CO_2, and methane. In the ethane pulse with no oxygen, a relatively high conversion to ethylene was obtained, probably due to both thermal decomposition and reaction with surface oxygen. Pulses of ethylene/O_2 (Fig. 8c) gave CO and CO_2 as the main products. In this case, the amount of carbon oxides produced was approximately three times larger than that obtained from ethane pulses, but only half of that obtained with methane pulses. CO oxidation produced CO_2 (not shown), even in pulses without oxygen, from the reaction of CO with surface oxygen. The results of these experiments (Figs. 8a, 8b, and 8c) indicate that ethylene can be produced in part by ethane dehydrogenation with lattice oxygen and that the main source of CO_x is the deep oxidation of either methane or methyl radicals on the catalyst surface (since blank experiments in the absence of the catalyst yielded negligible amounts of CO_x).

Further confirmation of the above results was obtained from additional experiments (not shown) performed using mass spectrometry to continuously monitor the exit products. The trace oxygen monitoring experiment, previously described for methane activation with lattice oxygen, was also carried out with ethane pulses, confirming that adsorbed oxygen reacts during dehydrogenation of ethane pulses over the 1.6Na/$NiTiO_3$ catalyst.

Mixtures of C_2H_6 with either $^{13}CH_4$ or CH_4 were reacted over the catalyst with the aim of identifying the origin of the CO_x species. Figure 9a shows the results obtained when pulses consisting of a mixture of 22% $^{13}CH_4$ (or CH_4, Fig. b), and 2.2% C_2H_6 and 8.9% oxygen in helium were reacted over the 1.6Na/$NiTiO_3$ catalyst. The methane conversion in these experiments was approximately 5%, which indicates that the maximum $^{13}C_2H_6$ concentration could be 0.55% in the hypothetic case of 100% selectivity. If CO_x was formed from the sequential reaction $^{13}CH_4 \rightarrow {}^{13}C_2 \rightarrow {}^{13}CO_x$ and from the deep oxidation of C_2H_6 added to the feed, the ratio $CO_2/^{13}CO_2$ would be approximately equal to 4 since this is the ratio of the maximum $^{12}C_2$ in the feed versus the maximum $^{13}C_2$. The result obtained in this experiment (Fig. 9a) is $CO_2/^{13}CO_2 = 0.7$, which indicates that a fraction of $^{13}CO_2$ was formed directly from $^{13}CH_4$, possibly from the direct oxidation of methyl radicals. The above is consistent with the results obtained using the pulse experiments with different amounts of oxygen (Fig. 8).

Catalyst characterization. In Table 2, the results of BET area measurements show that the total surface area decreases with increasing both Li and Na loading. Table 2 also lists X-ray diffraction results showing that the alkali-promoted catalysts are a complex mixture of several crystal phases. Table 3 summarizes the electron-binding energies of the elements detected on the Li and

TABLE 2

Surface Area and X-ray Diffraction Main Crystal Structures for the Alkali Metal-Promoted Nickel–Titanate Catalysts

Catalyst[a]	BET area (m^2/g)	XRD main phases
$NiTiO_3$	1.80	$NiTiO_3$, NiO
9.7% $Li/NiTiO_3$	0.88	$LiTiO_2$, $Li_2Ni_8O_{10}$
1.6% $Na/NiTiO_3$	1.70	$NiTiO_3$, NiO
22% $Na/NiTiO_3$	0.95	$NaTiO_2$, NiO

[a] After standard pretreatment.

sodium catalysts. The C1*s* and O1*s* spectra gave evidence that multiple carbon and oxygen species were present on the catalyst surface. Also included in Table 3 are the relative percentages of the integrated surface intensities of the oxygen species. The higher binding energy oxygen species relates to the presence of carbonate-type oxygen, and the various species exhibited by the C1*s* envelope have been associated with the following forms of carbon (*7*): (i) 284.6 corresponds to graphite or hydrocarbons; (ii) 287–288 eV could indicate C=O; carbonates are usually observed at 289 eV. Table 4 shows the surface composition as measured by XPS. Some sodium impurities were found on the surface of the lithium-promoted catalysts, most probably contained in the nickel titanate precursor. Interestingly, the percentage surface sodium on the $1.6Na/NiTiO_3$ catalyst is higher than the percentage surface lithium in the $9.7Li/NiTiO_3$ catalyst in spite of the lower loading of the former. It can also be observed in Table 4 that, while the ratio of Ni/Ti on the surface of the Li catalyst corresponds to the stoichiometry of the nickel titanate, for the Na-promoted catalyst the same ratio is between 1.44 and 2.10, which suggests the presence of nickel oxide on the surface of the sodium-promoted catalyst, in agreement with the XRD results (Table 2).

DISCUSSION

Despite the fact that both TiO_2 and NiO are very active catalysts in the deep oxidation of methane (*7, 23*), their combination in the ilmenite structure of $NiTiO_3$ results in an almost inactive catalyst. The unpromoted $NiTiO_3$ used in this study showed some segregation of both single oxides, but the low activity of this material suggests that these oxides are not exposed on the surface.

While it is well known that the addition of alkali metals to oxides promotes methane coupling, most previous results have been obtained at low loadings. We have shown that high loadings of either lithium oxide or sodium carbonate to the nickel ilmenate increased the hydrocarbon product yield, which for the catalysts studied in this work reached a maximum at lithium and sodium loadings of 9.7 and 22%, respectively. XRD analysis shows a decrease in the intensity of the $NiTiO_3$ lines when the percentage of alkali metal loading was increased, along with an increase in the intensities corresponding to NiO and $NaTiO_2$ for Na-loaded catalysts, and to $LiTiO_2$ and $Li_2Ni_8O_{10}$ crystalline phases in the case of lithium loading. Such morphological changes suggest that these new phases may be related to the increase in activity with increasing promoter loading.

The results obtained with the various transient techniques used in this work show that the role of the oxygen stored in the lattice varies depending on the type of promoter used and its loading. Thus, while the lattice oxygen is very active in methane coupling over the lithium-loaded catalyst, significant methane conversion occurs in the sodium-promoted catalysts only via weakly adsorbed oxygen. The results also suggest that the mobility of this lattice oxygen is fast at first (Fig. 5, first 10 pulses) but then becomes controlled by a slower diffusion process (Fig. 5, pulses 10–34). Eventually the rate of oxygen supply to the surface is not sufficient to prevent formation of surface Ni, thus giving rise to the loss in hydrocarbon selectivity (Fig. 5, pulse 35).

The causes for the different kinds of interaction between methane and oxygen when lithium- or sodium-promoted catalysts are used probably lies in the different chemical

TABLE 3

Electron Binding-Energy Results (eV)[a] for the Alkali Metal-Promoted Nickel–Titanate Catalysts

Sample	C1*s* (%)	O1*s* (%)	Ti2$p_{3/2}$	Li1*s*	Na1*s*	Ni2$p_{3/2}$
9.7% Li(f)	284.6 (70)	529.4 (62)	458	54.2		855.6
	289.6 (30)	531.7 (38)				
9.7% Li(r)	284.6 (65)	529.4 (58)	458	54.2		855.6
	289.8 (35)	531.6 (42)				
1.6% Na(f)	284.6 (56)	529.9 (82)	458.2		1072.5	856.1
	288.3 (21)	531.7 (18)				
	289.9 (17)					
	292.4 (6)					
1.6% Na(r)	284.6 (63)	529.9 (83)	458.3		1072.6	856.1
	288.5 (22)	531.7 (17)				
	290.3 (12)					
	292.6 (4)					
22% Na(f)	284.6 (26)	529.6 (40)	458.1		1072.6	855.9
	287.2 (12)	531.6 (60)				
	289.4 (51)					
	291.5 (11)					
22% Na(r)	284.6 (24)	529.7 (29)	458.2		1072.7	856.0
	287.0 (5)	531.5 (72)				
	289.4 (59)					
	291.5 (12)					

[a] Referenced against C1*s* line at 284.6 eV.

Note. f, Fresh sample; r, after 50 h of time-on-stream.

natures of the two alkali metals and their compounds. Since the ionic radius of lithium is smaller than that of sodium, the diffusion of lithium atoms into the ilmenite phase is favored. XRD analysis shows that while a mixed Li–Ni oxide is found for Li-loaded catalysts, no Na–Ni oxide is detected in the Na-loaded catalysts. That the surface concentration of Na found by XPS on the 1.6% Na-loaded catalyst is higher than the surface concentration of Li on the 9.7% Li-loaded catalyst suggests that lithium has a greater ability to diffuse into the bulk of the solid. Hatano and Otsuka (*24*) reported that lithium nickelate can activate methane in a redox cycle, which is in agreement with our results. Another physicochemical difference between the two promoters is their

TABLE 4

Surface Composition of the Alkali Metal-Promoted Nickel–Titanate Catalysts as Measured by X-Ray Photoelectron Spectroscopy

Sample	C	O	Ti	Li	Na	Ni	Ni/Ti
9.7% Li(f)	19.3	52.4	7.5	13.3	0.8	6.8	0.91
9.7% Li(r)	16.9	53.1	8.4	11.5	2.0	8.1	0.96
1.6% Na(f)	12.7	44.4	9.5	n.d.	19.6	13.7	1.44
1.6% Na(r)	12.1	45.3	9.4	n.d.	13.6	9.7	2.10
22% Na(f)	24.7	35.4	3.4	n.d.	28.8	5.8	1.71
22% Na(r)	24.9	35.4	2.8	n.d.	30.1	5.2	1.86

Note. f, Fresh sample; r, after 50 h of time-on-stream.

melting point, which is lower for the lithium carbonate (618°C) than for the sodium carbonate (850°C). Since XPS characterization revealed that the alkali metal on the surface is bonded to carbonate species, both fresh and after reaction, the presence of a quasi-liquid phase for the Li-promoted catalyst will favor an even distribution of the lithium promoter throughout the catalyst with respect to that of sodium.

As far as the methane interaction with the catalyst, the results of our transient experiments indicate that the concentration of long-lived adsorbed methane is too low to be differentiated from the interaction of Ar with the surface of both Li- and Na-promoted catalysts. This is in agreement with our previous attempts to measure methane adsorbed on Li/TiO_2 using the dynamic flow technique (*7*), and it has also been found to be the case for other oxidative coupling catalysts. On the other hand, Ekstrom and Lapszewicz (*25*) have measured the adsorption of methane on the surface of Sm_2O_3. These authors suggested that methane acts as a weak acid and the catalyst acts as a strong base. However, from their isotopic experiment they concluded that the adsorbed methane is not directly involved in the oxidative coupling reaction. However, Hatano and Otsuka (*24*) reported that the methane oxidative coupling reaction over lithium nickelate proceeds through the dissociation of the methane adsorbed over the catalyst surface. They arrived at that conclusion from deuterated methane experiments and also through the observation of a second order in the kinetics of methane oxidative coupling. Our kinetics analysis, presented in a subsequent paper (*19*), indicates that, in agreement with the transient results presented here, the kinetic results can also be interpreted via a redox mechanism for the Li-promoted catalyst and via a Eley–Rideal mechanism for the Na-promoted catalyst. Thus, in both cases the reaction pathway of methane is the same and the differences arise from the nature of the oxygen present on the surface.

The isotopic methane switch experiment also revealed that carbon dioxide interacts strongly with the basic surface of Li and Na catalysts under reaction conditions. Several reports indicate that this is a common characteristic of many active catalysts. Thus, Carreiro and Baerns (*26*) have made an attempt to correlate the basicity of the surfaces with the oxidative coupling activity; Ross *et al.* (*27*) suggested that the decomposition of the surface carbonates on a Li/MgO catalyst may lead to the formation of the active sites for the selective reaction. Taking into account these reports and the strong interaction of CO_2 with the basic surface of our catalysts, it is clear that the formation of carbonates must play an important role in the reaction. However, further investigation is required to provide definitive evidence concerning this point.

The results of pulse experiments with different feeds on the $1.6Na/NiTiO_3$ catalyst provide further understanding of the mechanism of C_2H_4 and carbon oxide formation. The most widely accepted mechanism of ethane formation in methane oxidative coupling appears to be the coupling of methyl radicals (*5*). However, reaction pathways like the formation of C_2H_4 and the nonselective reactions strongly depend on the type of catalyst used. Different mechanism have been proposed for C_2H_4 formation, including ethane dehydrogenation in the gas phase (*11*), direct formation from methane via methylene intermediates (*28*), and C_2H_6 dehydrogenation by reaction with lattice oxygen (*13*). In our transient experiments carried out with C_2H_6 plus oxygen pulses, little change in the concentration of the ethylene obtained was found when the oxygen concentration in the pulse was varied, in agreement with the results obtained by Asami *et al.* (*13*) for Pb/MgO catalysts. The trace oxygen monitoring experiment described under Results showed depletion of the oxygen concentration in the exit gas following the ethane pulse on the $1.6Na/NiTiO_3$ catalyst, which is a characteristic behavior when the catalyst is reduced. These results suggest that lattice oxygen may contribute to the dehydrogenation of ethane. However, it

is not clear from the above results whether ethane can directly reduce the oxide surface or whether the reduction takes place via the gaseous hydrogen formed from the thermal decomposition of ethane. Pulse experiments also showed that carbon monoxide can react with lattice oxygen to produce CO_2.

Is interesting to note that although the lattice oxygen of the sodium–nickel–titanate catalyst is not able to activate the methane molecule, the catalyst can be reduced with stronger reducing agents such as CO, H_2, and C_2H_6. Similar experiments performed with the $9.7Li/NiTiO_3$ catalysts showed that the solid can also be readily reduced with CO, H_2, or C_2H_6, in addition to the previously discussed reaction with methane. While kinetic experiments performed with different contact times (*19*) have shown that CO_2 and ethylene are secondary products formed from CO and ethane, the reducibility of the surface by ethane suggests that these secondary reactions can proceed through the reaction with lattice oxygen.

The mechanism of carbon oxide formation is another controversial point in the literature. Previous work on the Li/TiO_2 catalyst suggests that the oxidation of the hydrocarbon products in the gas phase is the main source of deep oxidation, thus imposing an intrinsic limitation in hydrocarbon yield. Results on La_2O_3 (*17*) indicate that although this catalyst is very effective in generating methyl radicals, it is also active in the total oxidation of C_2H_6. For the 1.6% sodium catalyst used in this work, transient experiments (Fig. 8) indicated that, although C_2 can be readily oxidized in the gas phase, the deep oxidation of methane or methyl radicals is the main source for CO_x formation. Also in pulses in which $^{13}CH_4 + C_2H_6 + O_2$ mixtures were fed, the main source of CO_2 production (in terms of total amount produced) was shown to be from $^{13}CH_4$ (Fig. 9).

CONCLUSIONS

The addition of Li and Na to $NiTiO_3$ promotes a rather inactive material into an active and selective catalyst for the oxidative coupling of methane. Transient experiments show that the role played by the different oxygen species (adsorbed, gas-phase, and lattice oxygen) strongly depends on the loading and the alkaline promoter used. Specifically, on a $9.7Li/NiTiO_3$ catalyst, the activity is related to lattice oxygen while gas-phase oxygen restores the consumed lattice oxygen rather than being directly consumed by the reaction. Conversely, there is little lattice oxygen involvement in oxidative coupling of methane over the Na-promoted catalyst (1.6 or 22% loading). These catalysts are almost inactive in the absence of gas-phase oxygen; however, their activity and selectivity increase significantly when the oxygen concentration is increased.

The different behaviors observed for both catalysts are related to the physicochemical properties of the two alkali promoters and their compounds formed with the nickel titanate support. These compounds affect the transfer of lattice oxygen and also exhibit different melting points depending on the alkali promoter used. While oxygen exhibits different pathways depending on the promoter used, the reaction pathway for methane was found to be the same for both alkali promoters. The route to deep oxidation products involves direct oxidation of methane or methyl radicals and, depending on the conditions used, the sequential oxidation of the C_2 hydrocarbon products.

ACKNOWLEDGMENTS

The financial support of Amoco Research Laboratories (Naperville, IL) is gratefully acknowledged. One of the authors (J.M.S) is grateful to the Direccion General de Investigacion Cientifica y Tecnica, Spain, for support as a Visiting Scholar.

REFERENCES

1. Bashin, M. M., *Stud. Surf. Sci. Catal.* **36,** 343 (1988).
2. Mimoun, H., *Nouv. J. Chim.* **11,** 513 (1987).
3. Ross, J. A., Bakker, A. G., Bosh, H., van Ommen, J. G., and Ross, J. R. H., *Catal. Today* **1,** 133 (1987).
4. Scurrell, M. S., *Appl. Catal.* **32,** 1 (1987).
5. Lee, J. S., and Oyama, S. T., *Catal. Rev. Sci. Eng.* **30**(2), 249 (1988).

6. Lane, G. S., and Wolf, E. E., *J. Catal.* **113,** 144 (1988).
7. Lane, G. S., Miro, E. E., and Wolf, E. E., *J. Catal.* **119,** 161 (1989).
8. Lane, G. S., Kalenik, Z., and Wolf, E. E., *Appl. Catal.* **53,** 183 (1989).
9. Driscoll, D. J., Martir, W., Wang J.-X., and Lunsford, J. H., *J. Amer. Chem. Soc.* **107,** 58 (1985).
10. Labinger, J. A., and Ott, K. C., *J. Phys. Chem.* **91,** 2682, (1987).
11. Iwamatsu, E., and Aika, K.-I., *J. Catal.* **117,** 416 (1989).
12. Miro, E. E., Santamaria, J. M., Kalenik, Z., and Wolf, E. E., *Catal. Today* **6,** 511 (1990).
13. Asami, K., Shikada, T., Fujimoto, K., and Tominaga, H.-O., *Ind. Eng. Chem. Res.* **26,** 2348 (1987).
14. Keller, G. E., and Bashin, M. M., *J. Catal.* **73,** 9 (1982).
15. Sofranko, J. A., Leonard, J. J., and Jones, C. A., *J. Catal.* **103,** 302 (1987).
16. Tagawa, T., and Imai, H., *J. Chem. Soc. Faraday Trans. 1* **84**(4), 923 (1988).
17. Lin, C. H. Campbell, K. D., Wang, J. X., and Lunsford, J. H., *J. Phys. Chem.* **90,** 534 (1986).
18. Otsuka, K., and Jinno, K., *Inorg. Chim. Acta* **121,** 237 (1986).
19. Miro, E. E., Santamaria, J. M., and Wolf, E. E., *J. Catal.* **124,** 465 (1990).
20. Lo, M.-Y, Agarwal, S. K., and Marcelin, G., *J. Catal.* **112,** 168 (1988).
21. Keulks, G. W., *J. Catal.* **19,** 232 (1970).
22. Happel, J., "Isotopic Assessment of Heterogeneous Catalysis." Academic Press, New York, 1986.
23. Otsuka, K., Liu, Q., Hatano M., and Morikawa, A., *Inorg. Chim. Acta* **118,** L23 (1986).
24. Hatano, M., and Otsuka, K., *J. Chem. Soc. Faraday Trans. 1* **85**(2), 199 (1989).
25. Ekstrom, J., and Lapszewicz, J. A., *J. Chem. Soc. Chem. Commun.*, 797 (1988).
26. Carreiro, J. A. S. P., and Baerns, M., *J. Catal.* **117,** 258 (1989).
27. Korf, S. J., Ross, J. A., de Bruijn, N. A., van Ommen, J. G., and Ross, R. H., *J. Chem. Soc. Chem. Commun.*, 1433 (1987).
28. Spinicci, R., *Catal. Today* **4,** 311 (1989).
29. Lin, C.-H., Wang, J.-X., and Lunsford, J. H., *J. Catal.* **111,** 301 (1988).